Studying Initiation and Growth of Shear Cracks in Reinforced Concrete Beams Using Full-Field Digital Imaging

Daniel C. Jansen, Assistant Professor
Department of Civil and Environmental Engineering
Tufts University
Medford, MA 02155

Sokhwan Choi, Senior Researcher
Korea Ocean Research and Development Institute (KORDI)
1270 Sa-dong, Ansan-si, Kyungi-do
Korea

Surendra P. Shah, Director
Center for Advanced Cement-Based Materials
Northwestern University
2145 Sheridan Road
Evanston, IL 60208

ABSTRACT

The mechanisms which lead to shear failure of longitudinally reinforced concrete beams are complex and often misunderstood. In this paper, a combination of a special closed loop test technique and machine vision are applied to tests on two reinforced concrete beams failing in shear: one made of normal strength concrete and the second of high strength concrete. To control the progression of the shear crack, a closed-loop test technique was devised and employed such that the crack propagation was stable even during the post peak. To locate the crack and to measure the crack displacements, machine vision, a nondestructive measuring technique, was employed which gives full-field displacements of a viewed area. The displacement measurements are obtained by first grabbing digital images of the observed area at different stages of loading during the test. By comparing discrete subsets of the reference and target images using normalized cross correlation matching, the displacement fields of the images are calculated. Shear crack initiation and progression are monitored for the two beams tested through

complete failure, and differences in the shear failures between reinforced beams made of normal and high strength concretes are noted.

INTRODUCTION

Thousands of tests have been performed on longitudinally reinforced concrete beams in shear during the past century, and hundreds of design equations have been proposed [1]. Most of these equations account for only the most basic mechanisms which induce failure or they are empirically based and do not account for the different mechanisms of shear resistance. Shear failure is a very complex combination of conditions which are still not fully understood.

Two primary sources which contribute to the lack of understanding of shear failures are that the mechanisms which lead to failure change depending on beam geometry and the brittleness of shear failures. The components which constitute shear resistance of longitudinally reinforced concrete beams can be roughly categorized as aggregate interlock, resistance of the compression zone, and dowel resistance of the reinforcement [2]. The final failure of the beam can be contributed to the loss of any one of these components. The amount which these mechanisms contribute to the overall resistance are dependent on one another and varies during the process of failure. These components are also functions of the beam's geometry such as the steel ratio, concrete strength, shear span ratio of the beam, and loading conditions. Shear failure is normally extremely brittle, and sudden, explosive failure results. Due to this brittleness, the progression of shear failure has not been documented. Often, several components resisting the shear force seemingly fail at once, which may lead to misdiagnosis of which mechanism actually leads to the final failure.

This paper describes a mechanical test method using closed loop control which can successfully obtain stable control of the test as the crack propagates even during the post-peak. During the tests which will be presented, digital images of the beam were captured, and full field displacement maps were made. This nondestructive method for obtaining the displacement maps is described. From these displacement maps, the crack location and width can be determined. The progression of the crack is described and the mechanisms leading to failure are presented.

EXPERIMENTAL DETAILS

Beam Setup

The beam test setup and geometry are given in Figure 1. The beams were tested in three point loading. Two grade 60 number 4 rebars (nominal yield strength of 470 MPa and diameter of 12.5 mm) were used as the reinforcing steel giving a steel ratio of 1.64%. Two different concrete strengths were used: normal strength concrete, f'_c = 39 MPa, and high strength concrete, f'_c = 108 MPa. The mix designs and concrete strengths are given in Table 1.

TABLE 1. Mix Designs and Compressive Strengths

Material (per m^3)	Normal Strength	High Strength
Cement (kg)	280	556
Silica Fume (kg)	-	54.5
Water (kg)	163.6	151.5
10 mm Pea Gravel, SSD (kg)	911	948
Fine Aggregate, SSD (kg)	1027	743
Superplasticizer (liters)	-	4.3
Total (kg)	2382	2457
W/C	0.58	0.27
W/(C + Silica Fume)	0.58	0.25
f'_c, 28 days (MPa)	34.8 ± 0.2	97.2 ± 1.6
f'_c, at time of beam test (MPa)	38.7 ± 0.5	107.9 ± 2.9

External stirrups were placed on the east span of the beam, as shown in Figure 1, in order to force the shear failure to occur on the west span. The reference frame was fixed to the center of the beam directly under the load point, shown in Figure 2, such that if the center of the beam rotates, then the frame rotates with it. An LVDT with a range of ± 12.5 mm was attached to the reference frame at the point of the west end beam support and measured the displacement of the west span only. This configuration created the boundary conditions for the displacement of the load point identical to the displacement of the cantilevered beam shown in Figure 2. This displacement will be referred to as DispW. LVDTs were placed vertically on the rear face of the beam in the configuration as shown in Figure 1 and are labeled V1 through V7. LVDTs V1 and V2 had ranges of ±7.5 mm, V3 and V4 had ranges of ±5 mm, and V5 through V7 were ±2.5 mm. The front surface of the west span of the beam was left unobstructed so it could be viewed by the CCD camera taking capturing the images. A fine layer of the viewed surface was ground off the beam to expose the aggregates which gives a random pattern necessary for the image cross correlation technique described in the following section.

The feedback signal to control the test was a linear combination of measured displacements in mm:

$$\text{Feedback} = \text{DispW} + 3(V2+V4+V6) \quad (1)$$

This signal was digitally calculated by the computer controlling the test machine. For control of this particular test setup and geometry, this combination for the feedback control was found to give optimum control of the test. Optimum control is considered to be when slow stable control is obtained during the post-peak and the initial loading rate is not too fast. Since snapback was observed in the Force vs. DispW curve, the vertical LVDTs control the stability of the test during the post-peak; however, DispW dominated the feedback signal during the pre-peak before the shear crack initiated and the vertical LVDTs had not begun to measure any displacement. The feedback signal was increased monotonically at a rate of .0213 mm/second which gave a total test time of a little more than an hour. The

advantage of using multiple LVDTs as feedback is that the opening of the crack is captured regardless of the exact crack location which is not known prior to testing. Also, as the crack extends and grows, there is always a vertical LVDT near the crack tip.

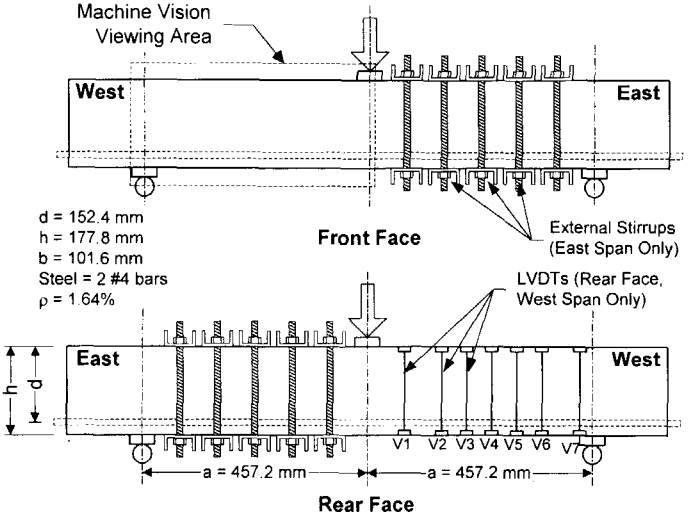

Fig. 1 Beam Test Setup

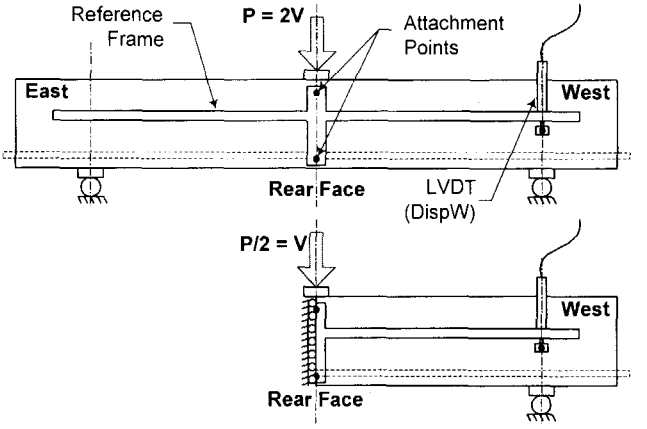

Fig. 2 Reference Frame and Symmetry

Machine Vision

Digital image analysis has been used for measuring displacements in different applications [3,4,5,6]. For the study of shear crack detection in reinforced concrete beams, digital image analysis was adopted and presented in this paper. There are several advantages in using the current measuring method. Unlike conventional measuring methods, this one does not require direct attachment of gages on specimens. This means that possible disturbances of the gage readings during a test can be avoided. Also since there is no limit for the size of a specimen, a practical testing size can be chosen such as reinforced concrete beams.

Measurement based on digital image analysis, often called computer vision, uses normalized cross correlation function to define the level of resemblance in a pair of images. The correlation coefficient, r(m,n), is defined as

$$r(m,n) = \frac{N\sum_i\sum_j T'R' - \sum_i\sum_j T' \sum_i\sum_j R'}{\left[N\sum_i\sum_j [T']^2 - \left[\sum_i\sum_j T'\right]^2\right]^{\frac{1}{2}} \left[N\sum_i\sum_j [R']^2 - \left[\sum_i\sum_j R'\right]^2\right]^{\frac{1}{2}}} \quad (2)$$

where R' and T' are the pixel intensities of the target image at pixel location (i,j) and the reference image at pixel location (i-m,j-n), respectively [6,7]. Pixel intensities are based on the gray scale level being measured, ranging from 0 (black) to 255 (white). r(m,n) is the mormalized cross correlation which has values from 0 (no match) to 1 (perfect match) By maximizing the correlation coefficient, r(m,n), the displacements (m,n) can be obtained.

Since conventional photographic films and papers introduce undesired distortions on images during chemical processing and to eliminate the time consuming step of photographic processing, a digital CCD camera was used to grab images at different loading stages. The camera was mounted on a heavy I-beam to reduce vibrations from the hydraulic testing machine. The surface of testing beam was ground to expose the aggregate. This gives better image contrast which is necessary for accurate measurement with the image cross correlation technique.

A series of images were stored on a host computer during the test at different stages of crack growth. Each image consisted of the gray level (0 to 255) over a total area of 1280 X1024 pixels. For the beams tested in this investigation, the area corresponding to the beam surface under investigation was 1280 X 510 pixels. Processes from image recording to post analyses were automated through developed computer programs. Any pair of images can be used to measure the amount of relative displacements occurring between those two images. The displacements were measured at a spacing of ten pixels, or at 6528 (128 X 51) nodes uniformly distributed over the image areas. Each image subset used to calculate the displacement at a node consists of an area 24 X 24 pixels, subsequently there is some overlap of the image subset used to calculate the displacement at adjacent nodes. For this investigation, image 0, captured before

load was applied, is compared to images captured at different stages of loading, giving the displacement maps at each loading stage.

The measurement errors calibrated based on image shifting is estimated to be about .02 pixels for the mean value, and about .04 pixels for the standard deviation. For the case being examined here, 1 pixel corresponds to .386 mm; subsequently, the accuracy could be as high as .0075 mm for the mean value and .015 mm for the standard deviation. The actual measuring accuracy is affected by the quality of the images. Also, the larger the area being examined, the larger the errors.

Displacement fields were successfully obtained between the unloaded reference image and selected images which represent different loading stages and, consequently, shear crack opening stages.

TEST RESULTS

This section describes the results obtained from the testing of the beams described earlier and is divided into three subsections: the first describes the results from the mechanical testing of the beams, the second gives a description the results obtained using machine vision, and the third correlates the results of the shear vs. DispW curves with crack extension obtained using machine vision.

Results from Mechanical Testing

The shear force versus displacement curves for DispW and the feedback signal are shown in Figure 3. Note that snapback occurs in the force-DispW curve for the beam made of high strength concrete which means that if DispW was used as the feedback alone, then control of the test after the peak would not have been maintained. The difference between the DispW and feedback curves in Figure is the component of the feedback signal measured by the surface LVDTs, 3(V2+V4+V6), given in equation 1.

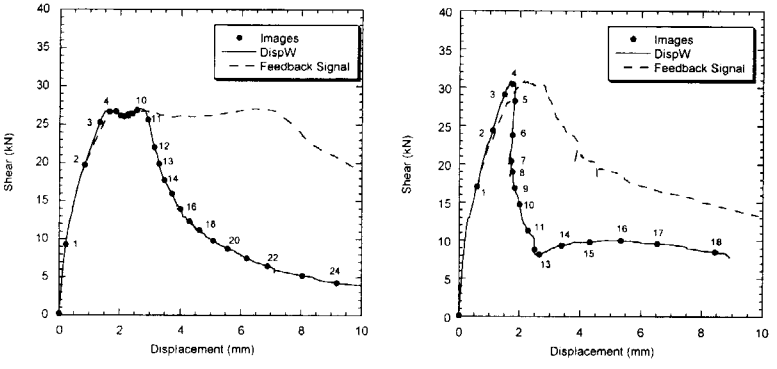

a) Normal Strength b) High Strength

Fig. 3 Shear vs. Displacement Curves

Stroke (displacement of the hydraulic loading piston) is commonly used for feedback control for this type of test; however, severe snapback occurred in the load vs. stroke curve (not shown) which explains the usual explosive nature of shear failures. The beam made of high strength concrete failed in a more brittle manner than the similar beam of normal strength concrete. This may be partially offset by the fact that this beam is relatively small compared to full scaled structural members; due to size effects smaller structures behave in more ductile fashion than their larger counterparts.

Results from Machine Vision

Images were captured with the CCD camera at all the points along the shear-displacement curve as shown in Figure 3. Figures 4 and 5 show the u and v contours for the beams made of normal and high strength concrete for the image points given in Figure 3. The u and v contours are the displacements in the x and y directions respectively. When contour lines are close together and are not evenly spaced, this indicates non-uniform strain or rigid body displacement or rotation, indicating the concrete is cracked.

Correlation between Shear-DispW Curves and Machine Vision Results

Prior to the peak load for the normal strength beam, three distinct flexural cracks bending towards the load point can be seen in Image 3 in Figure 4a. It was after the first peak that the third flexural crack from the load point became the critical shear crack and vertical opening of the shear crack can be seen in Image 4 in Figure 4a. Similarly, the high strength beam had no vertical displacement of the shear crack just prior to the peak load; however, at the peak, significant vertical displacement of the shear crack can be seen (Images 3 and 4 in Figure 5a).

Just after the peak load with the high strength beam, debonding of the rebar can be visually seen in Image 5 of Figure 5a in the form of a secondary crack just behind the primary shear crack. It may also be possible that this secondary crack could have been initiated by dowel action. Similar cracking was observed with the normal strength beam, although it was simply splitting along the rebar without the secondary crack. More significant however, there was no drop in load with the normal strength beam even though splitting had occurred quite a distance along the rebar as can be seen in Image 10 in Figure 4a.

For the high strength beam, significant drop in load is observed as the shear crack propagates to the load point and continued splitting occurs along the rebar as can be seen from Images 8 and 10 in Figure 5b. Some increase in the load carrying capacity of the high strength beam is observed after Image 13 in Figure 3 which corresponds to the point at which the splitting along the rebar reaches the support (Image 13, Figure 5b); this increase is due to the arrest of the splitting due to the closing force provided by the support.

The second peak is reached with the normal strength beam as the compression zone fails at the head of the shear crack which can be seen by comparing Images 10 and 11 in Figures 4a and 4b. The continued drop in load for this beam corresponds to progressing dowel splitting along the rebar (Image 16, Figure 4b).

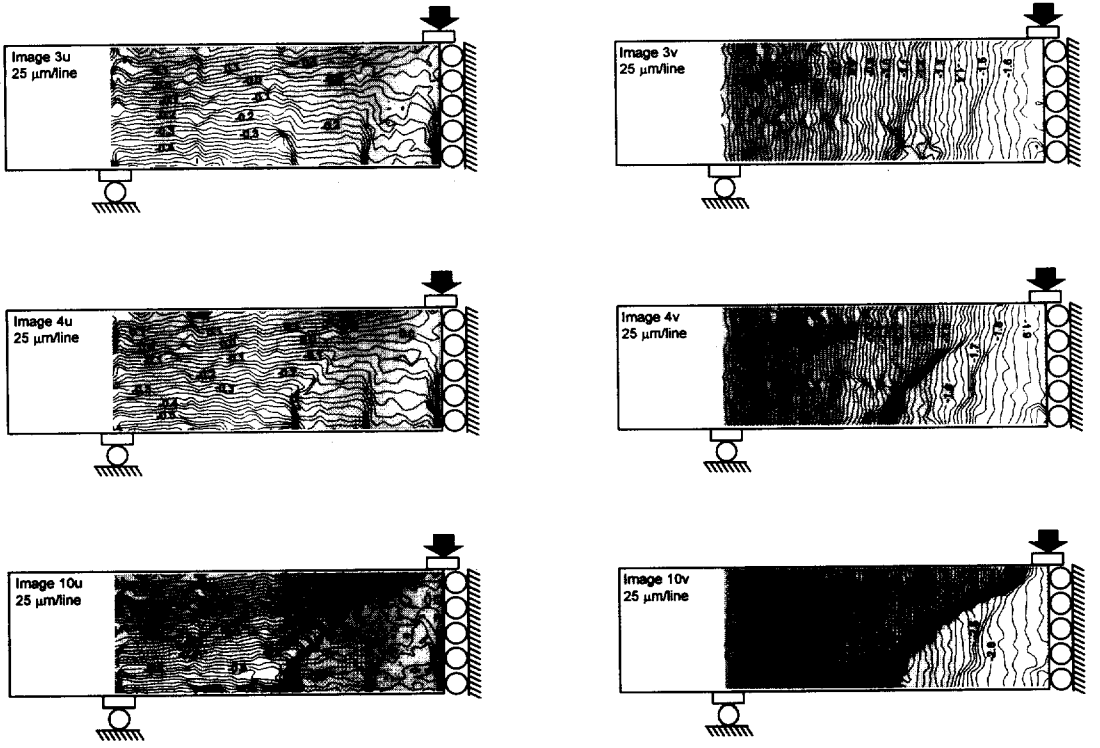

Fig. 4a Displacement Contours for Normal Strength Beam - Images 3, 4, and 10

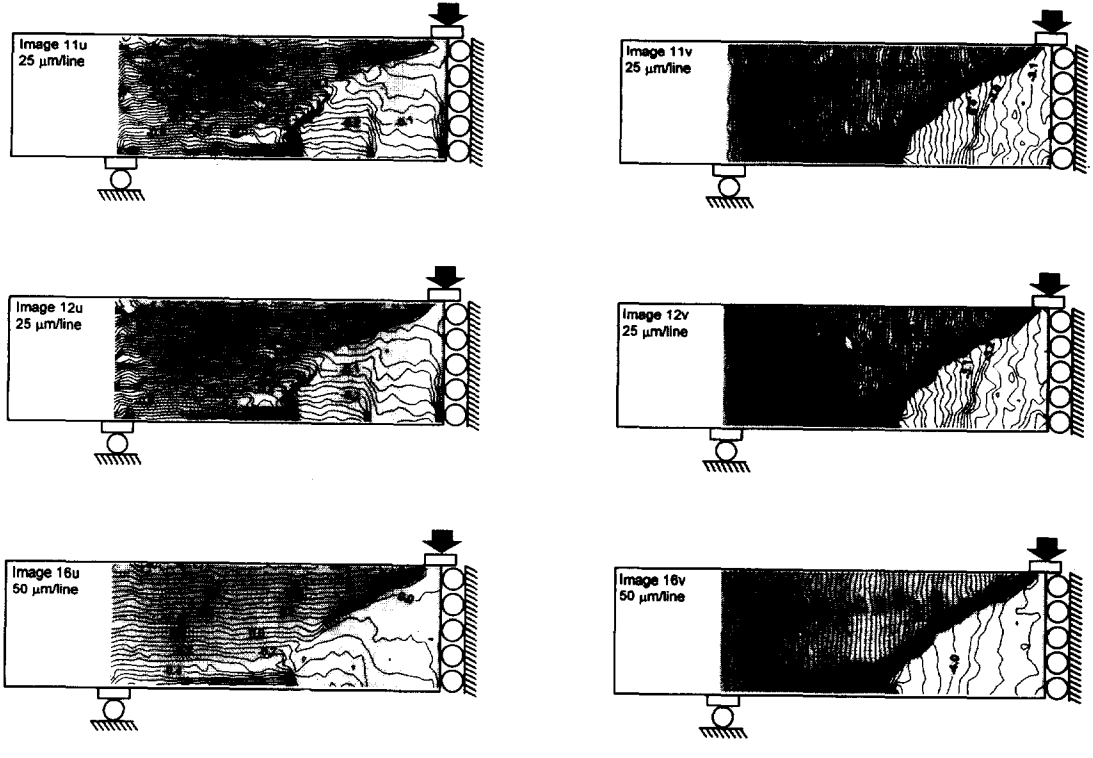

Fig. 4b Displacement Contours for Normal Strength Beam - Images 11, 12, and 16

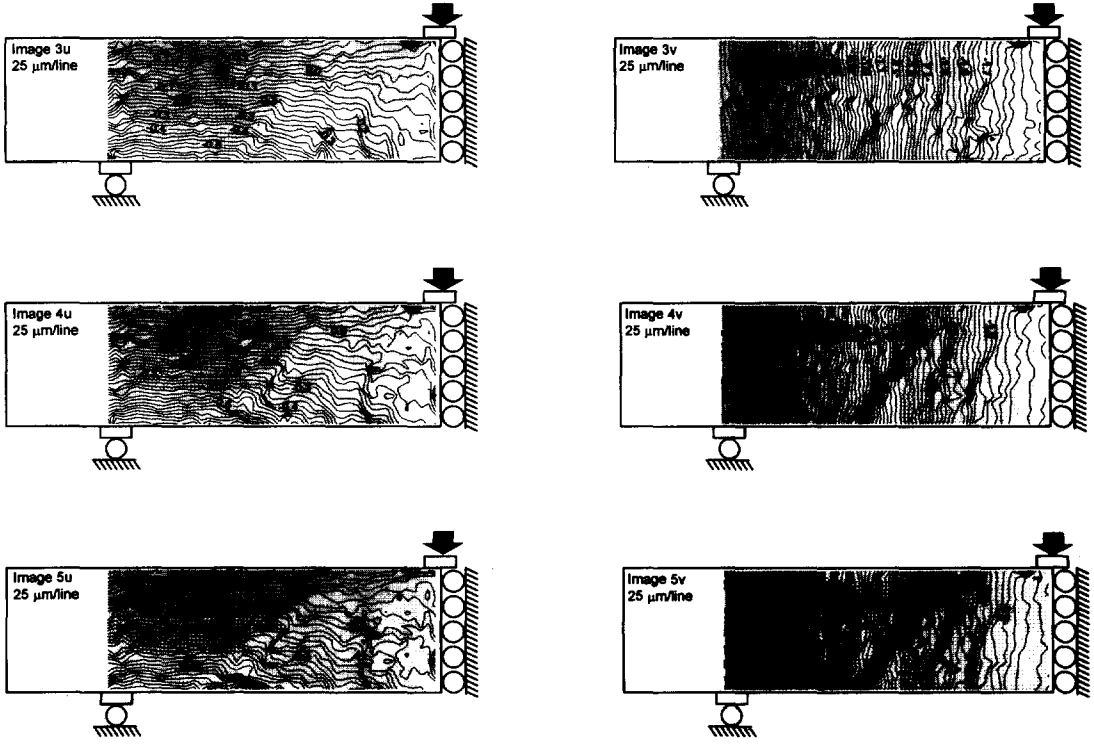

Fig. 5a Displacement Contours for High Strength Beam - Images 3, 4, and 5

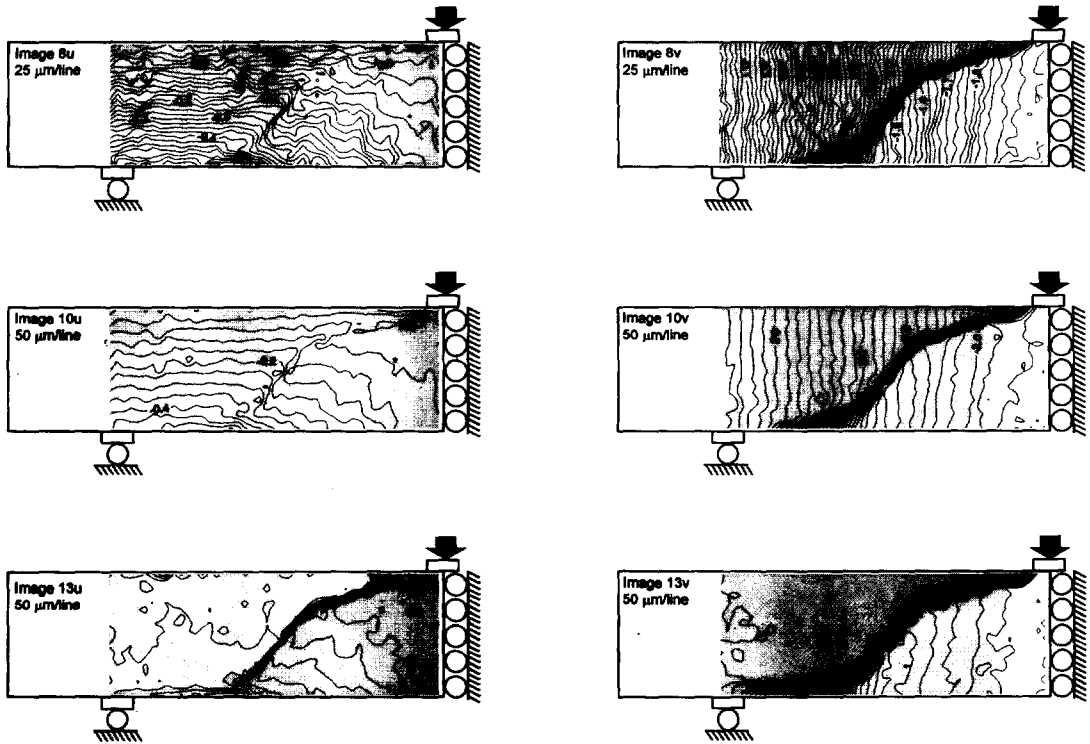

Fig. 5b Displacement Contours for High Strength Beam - Images 8, 10, and 13

Discussion of Results

From the displacement fields, smaller areas can also be examined. In order to determine the opening and sliding of the shear crack, the displacements at a series of nodes on opposite sides of the final shear crack need to be examined [8]. To perform this analysis, the local rotation of the beam due to bending must be accounted for, then the relative x and y displacements of the opposing nodes can be calculated. Using the angle of inclination of the shear crack, vector displacements along the crack can be separated into sliding and opening displacements. From the opening and sliding displacements, the amount of resistance provided by aggregate interlock can be calculated using one of a number of existing models which relate these displacements into normal and shear stresses for normal strength concrete [9, 10] and high strength concrete [11]. This analysis is presented elsewhere [8].

CONCLUSIONS

In this investigation, longitudinally reinforced concrete beams made of normal and high strength concretes were tested using closed-loop feedback control. A method for obtaining stable control throughout the test was described and implemented. Machine vision, a method to obtain full-field displacements was described and applied during the testing of the beam. From the data produced, the progression of shear failure for reinforced beams made of normal and high strength concretes has been described as initiation of flexural cracks prior to peak followed by the failure of the bond between the rebar and concrete which occurs at the peak load. The load carrying capacity of the high strength beam diminishes rapidly as splitting continues along the rebar until it reaches the reaction. For the normal strength beam, the load is sustained even as dowel splitting takes place, and the load carrying capacity only diminishes once the compression zone ruptures. The value of application of computer vision has been shown to be enormous due to its relative simplicity and robustness.

ACKNOWLEDGMENTS

The authors thank the National Science Foundation Center for Advanced Cement-Based Materials and the Illinois Technological Challenge Grant for funding of the research presented here. The first author would also like to thank the Department of Civil and Environmental Engineering at Tufts University and the Engineering Foundation for sponsorship at this conference.

REFERENCES

[1] Collins, M. P., Mitchell, D., Adebar, P., Vecchio, F. J., "A General Shear Design Method," *ACI Structural Journal*, Vol. 93, No. 1, Jan.-Feb. 1996, pp. 36-45.

[2] Park, R., Paulay, T., Reinforced Concrete Structures, A Wiley Interscience Publication, John Wiley and Sons, New York,1975, pp. 769.

[3] Franke, E. A., Wenzel, D. J. and Davidson, D. L. (1991). "Measurement of microdisplacements by machine vision photogrammetry (DISMAP)." *Rev. Sci. Instrum.*, Vol. 62, No. 5, pp. 1270-1279.

[4] Goshtasby, A., Turner, D. A. and Ackeman, L. V. (1992). "Matching of tomographic slices for interpolation." *IEEE trans. on Medical Imaging*, Vol. 11, No. 4, pp. 507-516.

[5] Sutton, M. A., Turner, J. L., Chao, Y. J., Bruck, H. A. and Chae, T. L. (1992). "Experimental investigations of three-dimensional effects near a crack tip using computer vision." *International Journal of Fracture*, Vol. 53, pp. 201-228.

[6] Choi, S., "Fracture Mechanism in Cement-Based Materials Under Compressive Loads," Ph.D. Dissertation, Northwestern University, Evanston, IL, 1996.

[7] Pratt, W. K., Digital Image Processing, 2nd edition, A Wiley-Interscience Publication, John Wiley & Sons, Inc, 1991.

[8] Jansen, D. C., "Postpeak Properties of High Strength Concrete Cylinders in Compression and Reinforced Beams in Shear," Ph.D. Dissertation, Northwestern University, Evanston, IL, 1996, 224 pp.

[9] Bazant, Z. P., and Gambarova, P., "Rough Cracks in Reinforced Concrete," *Journal of the Structural Division*, ASCE, Vol. 106, No. ST4, April 1980, pp. 819-842.

[10] Walraven, J. C., "Fundamental Analysis of Aggregate Interlock," *Journal of the Structural Division*, ASCE, Vol. 107, No. ST11, Nov. 1981, pp. 2245-2270.

[11] Walraven, J. C., and Stroband, J., "Shear Friction in High Strength Concrete," High Performance Concrete, Proceedings, SP-149, ACI International Conference, Singapore, 1994, pp. 311-330.